

Bayesian inference on Brain-Computer Interface using the GLASS Model

Bangyao Zhao

Department of Biostatistics, University of Michigan

and

Jane E. Huggins

Department of Physical Medicine and Rehabilitation and

Department of Biomedical Engineering, University of Michigan

and

Jian Kang

Department of Biostatistics, University of Michigan

April 18, 2023

Abstract

The brain-computer interface (BCI) enables individuals with severe physical impairments to communicate with the world. BCIs offer computational neuroscience opportunities and challenges in converting real-time brain activities to computer commands and are typically framed as a classification problem. This article focuses on the P300 BCI that uses the event-related potential (ERP) BCI design, where the primary challenge is classifying target/non-target stimuli. We develop a novel Gaussian latent group model with sparse time-varying effects (GLASS) for making Bayesian inferences on the P300 BCI. GLASS adopts a multinomial regression framework that directly addresses the dataset imbalance in BCI applications. The prior specifications facilitate i) feature selection and noise reduction using soft-thresholding, ii) smoothing of the time-varying effects using global shrinkage, and iii) clustering of latent groups to alleviate high spatial correlations of EEG data. We develop an efficient gradient-based variational inference (GBVI) algorithm for posterior computation and provide a user-friendly python module available at <https://github.com/BangyaoZhao/GLASS>. The application of GLASS identifies important EEG channels (PO8, Oz, PO7, Pz, C3) that align with existing literature. GLASS further reveals a group effect from channels in the parieto-occipital region (PO8, Oz, PO7), which is validated in cross-participant analysis.

Keywords: Bayesian Analysis; Latent Group; Multinomial Regression; Gaussian Process

1 Introduction

A brain-computer interface (BCI) facilitates direct communication between a user and a computer by interpreting brain-generated signals. BCIs have shown great potential in helping individuals with severe physical impairments such as amyotrophic lateral sclerosis (ALS) to communicate with the outside world. Recent research has concentrated on the P300 BCI application, utilizing scalp electroencephalography (EEG) to record brain activity. This method utilizes the event-related potential (ERP) BCI design, first proposed by Farwell & Donchin (1988). ERPs are electrical signals generated in response to external stimuli. The P300 ERP exhibits a positive amplitude peak approximately 300 milliseconds after the stimulus; hence it has the name “P300” response.

Figure 1 illustrates the ERP-BCI design. During the task, the participant is instructed to focus on a specific character (referred to as the target character) displayed on a virtual keyboard, typically arranged in a 6×6 grid. The six rows and six columns on the virtual keyboard will flash randomly, with each flash considered as a stimulus. The presentation of 12 stimuli is called a sequence. Each sequence comprises one flash of every row and column, resulting in two target stimuli and ten non-target stimuli. The participant is instructed to mentally respond upon observing a target stimulus, either by counting the target stimuli or simply saying “yes” mentally. Physical responses, such as button presses, are not required, and the computer relies solely on EEG signals to determine the target character.

The foundational computational neuroscience challenge in ERP BCIs lies in accurately classifying each stimulus as either a target or a non-target. Correct binary classification allows for the precise identification of the target row, the target column, and, ultimately, the target character at their intersection. In practice, an interval (typically 800 milliseconds) of the EEG signal is extracted following the onset of each stimulus (see Figure 2). Features



Figure 1: Illustration of a P300-speller. The screen displays a 6×6 virtual keyboard. The rows and columns of the virtual keyboard are flashing at random. The flashing of one row or one column is considered a stimulus to the participant. In this example, the participant has typed “THE QUICK” and intends to type the next target character “Sp” (space), which is located at the intersection of row 5 and column 3. The current stimulus is on column 3, so it is a target stimulus. The participant responds by saying “yes” mentally. The computer records the participant’s real-time EEG signal through electrodes to determine whether the current stimulus is a target.

within the extracted EEG series are then employed to predict the binary stimulus type (target/non-target), which effectively formulates the task as a standard binary classification problem. With a well-calibrated classification model, generating a new 12-stimuli sequence and identifying the two target stimuli enables the typing of a new character.

The classification of P300 stimuli in ERP BCIs poses several challenges. First, EEG signals are commonly sampled at high frequencies and captured by multiple channels, leading to a high-dimensional feature space. For example, a typical EEG recording at 256 Hz during an 800-millisecond interval generates 205 time points, and with a 16-channel EEG cap, the feature space dimension increases to $205 \times 16 = 3280$. Second, scalp EEG signals have a high spatial correlation due to the conductive properties of the skull and brain tissues. Also, these signals also exhibit high temporal correlation as they reflect the continuous neural activity of the brain. The presence of high correlations may lead to overfitting problems. Third, the amplitude of the P300 component is typically small compared

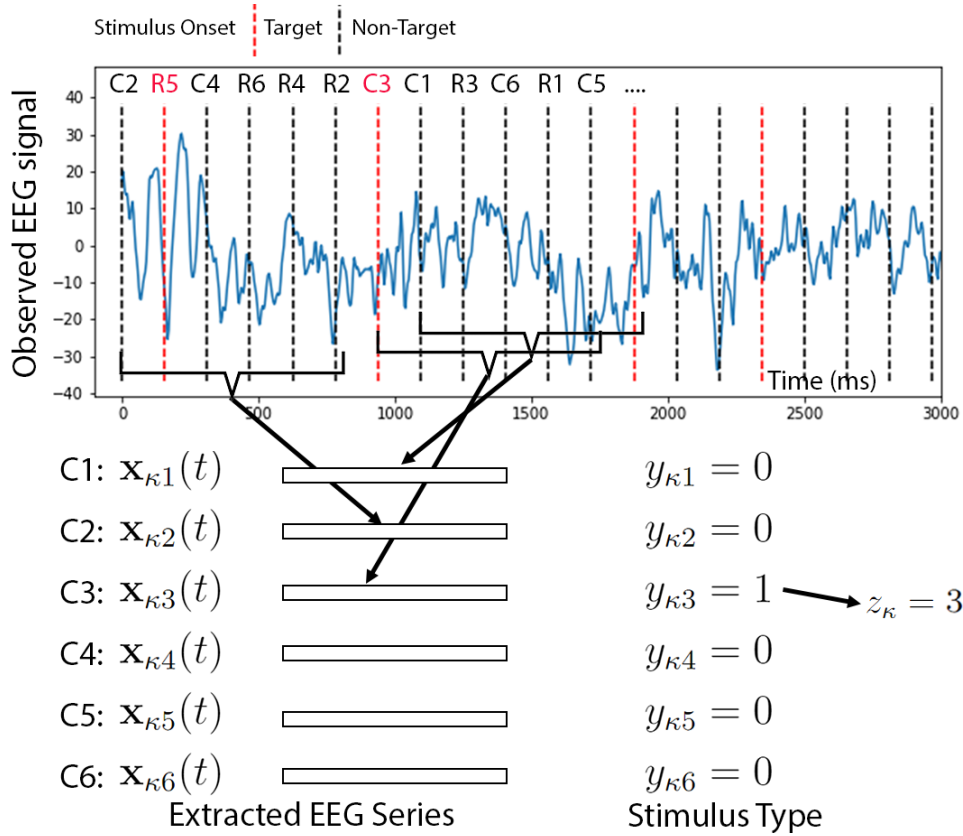


Figure 2: Illustrations of a 12-stimuli sequence accompanied by the real-time EEG signal. The labels “C3 R5 C4 ...” (column 3, row 5, column 4, ...) at the top represent the order of stimuli presentation, which is a permutation of the rows and columns of the virtual keyboard with dimensions 6×6 . In this example, the target character is located at the intersection of row 5 and column 3. An 800 ms EEG series is extracted after each stimulus. Conventional classification frameworks make independent predictions of the binary stimulus type using the extracted EEG series. However, in GLASS, one target stimulus is chosen from every six stimuli, which distinguishes GLASS from traditional frameworks. The figure illustrates the EEG series extraction of the six stimuli on columns, which we call a half-sequence. Further details regarding the notations in this figure can be found in Section 2.

to background EEG activity, resulting in a low signal-to-noise ratio (SNR). Furthermore, the study design includes only two target stimuli within a 12-stimulus sequence, resulting in an imbalanced dataset.

The original work on P300 BCI (Farwell & Donchin 1988) tested four classification methods, where the stepwise linear discriminant analysis (SWLDA) achieves the best performance. Following the original work, numerous methods have been proposed in this field, aligning with trends in method development. Krusienski et al. (2006) compared five state-of-the-art methods at that time, including Pearson’s correlation method (PCM), Fisher’s linear discriminant (FLD), SWLDA, linear SVM (LSVM), and Gaussian kernel SVM (GSVM). This study showed that SWLDA and FLD provide the best overall performance and implementation characteristics, highlighting SWLDA’s feature selection ability. Philip & George (2020) did a comprehensive review of 42 articles related to classification methods in P300 BCIs, reporting that most methods fell into three categories: ensemble learning (24%), SVM (24%), and discriminant analysis (43%). Since 2018, an increasing number of neural network-based approaches have emerged, including a compact convolutional neural network called EEGnet (Lawhern et al. 2018), a convolutional long short-term memory (ConvLSTM) model (Joshi et al. 2018), and a multi-task autoencoder-based model (Ditthapron et al. 2019). Most current ERP BCI classification methods adopt the binary classification framework, which does not take into account the intrinsic data-generating process in P300 BCI design. Ma et al. (2022) is one exception, which adopts a Bayesian generative model to model EEG patterns using the Gaussian process prior. However, their work focuses on interpreting brain signals rather than classification.

This article proposes a novel Bayesian approach for P300 BCI classification: the Gaussian latent group model with sparse time-varying effects (GLASS). GLASS is built upon a

constrained multinomial logistic regression model that fundamentally differs from existing binary classification methods. GLASS provides a model-based solution to the row-column paradigm of P300 BCI by directly selecting the target stimulus from a half-sequence, which consists of the six stimuli corresponding to either rows or columns. Thus, a 12-stimuli sequence comprises two 6-stimuli half-sequences, each containing one target stimulus and five non-target stimuli. Under a Bayesian modeling framework, we develop several novel prior specifications of model parameters. First, we construct a Gaussian latent group decomposition of the time-varying regression coefficients through a group indicator and a projected normal distribution. With this decomposition, the spatially correlated EEG signals across channels are formed into several latent groups, which can be interpreted as signals at latent channels in the multinomial logistic regression model. The latent group decomposition retains most of the information of the original EEG channels while reducing the spatial correlations among latent channels. Second, we adopt the soft-thresholding prior for the time-varying coefficients to impose sparsity and employ the global shrinkage prior on the difference in coefficients between the adjacent time points. For posterior computation, we utilize a gradient-based variational inference (GBVI) method to estimate the posterior distribution of model parameters and simulate the posterior predictive distribution of the target stimuli. Additionally, we propose a model-based evaluation of EEG channel importance using Bayes factors.

The remainder of the article is organized as follows. Section 2 develops the GLASS model and prior specifications, as well as the GBVI algorithm for posterior computation. Section 3 presents analysis of BCI data using GLASS in comparisons to existing methods. Section 4 performs extensive simulations to demonstrate the classification accuracy and robustness of GLASS. Finally, Concluding remarks are given in Section 5.

2 Method: GLASS

We begin by introducing necessary notations. Let l ($l = 1, \dots, L$) index characters, and for each character suppose there are J sequences (indexed by j ($j = 1, \dots, J$)). Each sequence contains two half-sequences (indexed by $s = 1, 2$) corresponding to the six row stimuli (denoted by $s = 1$) and six column stimuli (denoted by $s = 2$). The six stimuli in one half-sequence are indexed by i ($i = 1, \dots, 6$). To reduce notation complexity, we define an index set $\mathcal{K} = \{(l, j, s) \mid l = 1, \dots, L; j = 1, \dots, J; s = 1, 2\}$ with every $\kappa \in \mathcal{K}$ uniquely determining a half-sequence. For example, $\kappa = (2, 3, 1)$ uniquely identifies the row half-sequence in the third sequence generated for the second character. If one further knows $i = 4$, it refers to the stimulus on the fourth row. We use $\mathbf{x}_{\kappa i}(t) = \{x_{\kappa i 1}(t), \dots, x_{\kappa i E}(t)\}^\top \in \mathbb{R}^E$ to denote the E -channel (indexed by e ($e = 1, \dots, E$)) EEG time series following stimuli (κ, i) . In practice, we observe n_T evenly spaced time points $\{0 = t_1 < t_2 < \dots < t_{n_T} = t_{max}\}$. These time points are indexed by p ($p = 1, \dots, n_T$). Usually, $t_{max} = 800$ milliseconds, and n_T depends on the sampling frequency. Let $y_{\kappa i}$ denote the stimulus type (target as 1 and non-target as 0), and z_κ ($z_\kappa \in \{1, \dots, 6\}$) denote the index of target stimuli in the half sequence κ . The event $\{z_\kappa = i\}$ is equivalent to $\{y_{\kappa i} = 1, y_{\kappa j} = 0, j \neq i\}$.

2.1 Constrained Multinomial Logistic Regression Model

We specify the probability distribution of the i th stimulus being the target in half sequence κ , i.e. $z_\kappa = i$, given the three dimensional EEG array $\mathbf{X}_\kappa = \{x_{\kappa i e}(t_p) : i = 1, \dots, 6; e = 1, \dots, E; p = 1, \dots, n_p\}$.

$$\Pr(z_\kappa = i) = \frac{\exp(\eta_{\kappa i})}{\sum_{i'=1}^6 \exp(\eta_{\kappa i'})} \quad \text{with} \quad \eta_{\kappa i} = \sum_{p=1}^{n_T} \mathbf{x}_{\kappa i}^\top(t_p) \boldsymbol{\beta}(t_p), \quad (1)$$

where $\boldsymbol{\beta}(t) = \{\beta_1(t), \dots, \beta_E(t)\}^\top$ is the E -dimensional time-varying effects with $\beta_e(t)$ denoting the effect of EEG channel e . In (1), the probability of $z_\kappa = i$ is linked to $\eta_{\kappa i}$ through a softmax function, and $\eta_{\kappa i}$ is interpreted as the un-normalized log odds of being the target.

The formulation of a general multinomial regression framework is $\eta_{\kappa i} = \sum_{i'=1}^6 \sum_{p=1}^{n_T} \mathbf{x}_{\kappa i'}^\top(t_p) \boldsymbol{\beta}_{i i'}(t_p)$, of which (1) is a constrained version, i.e., $\boldsymbol{\beta}_{i i'}(t) = \mathbf{0}$ if $i \neq i'$ and $\boldsymbol{\beta}_{11}(t) = \dots = \boldsymbol{\beta}_{66}(t) = \boldsymbol{\beta}(t)$.

2.2 Prior Specifications

2.2.1 Latent Group Decomposition of Time-varying Effects

We introduce a latent group decomposition of time-varying effects $\beta_e(t)$ for $e = 1, \dots, E$,

$$\beta_e(t) = \sum_{h=1}^H \delta_{eh} \alpha_{eh} \tilde{\beta}_h(t), \quad (2)$$

where H is a pre-specified number of latent groups. For $h = 1, \dots, H$, $\delta_{eh} \in \{0, 1\}$ is a latent group indicator to specify whether channel e contributes to latent channel h , and $\alpha_{eh} \in [-1, 1]$ is the contribution weight from channel e to latent channel h . The time-varying coefficient $\tilde{\beta}_h(t)$ represents the effects from the latent channel h . To ensure the identifiability, we assume that each EEG channel is only allowed to contribute to one latent channel, i.e., $\sum_{h=1}^H \delta_{eh} = 1$ and the contributing weights are normalized with the L_2 norm, i.e. $\sum_{h=1}^H \alpha_{eh}^2 = 1$.

With (2), the EEG signals at all E channels can be summarized into H latent channels. The log odds of the target stimulus $\eta_{\kappa i}$ in (1) can be re-expressed as a linear function of EEG signals at the latent channels as follows:

$$\eta_{\kappa i} = \sum_{p=1}^{n_T} \tilde{\mathbf{x}}_{\kappa i}^\top(t_p) \tilde{\boldsymbol{\beta}}(t_p) \quad \text{with} \quad \tilde{x}_{\kappa i h}(t) = \sum_{e=1}^E \delta_{eh} \alpha_{eh} x_{\kappa i e}(t), \quad (3)$$

where $\tilde{\mathbf{x}}_{\kappa i}(t) = \{\tilde{x}_{\kappa i1}(t), \dots, \tilde{x}_{\kappa iH}(t)\}^\top$ represents the summarized EEG signals at H latent channels depending on δ_{eh} and α_{eh} , and $\tilde{\boldsymbol{\beta}}(t) = \{\tilde{\beta}_1(t), \dots, \tilde{\beta}_H(t)\}^\top$ is the time-varying effects of the corresponding latent channels, or called the group-level time-varying effects.

2.2.2 Soft-thresholding with Global Shrinkage Prior

We propose a soft-thresholding with global shrinkage prior for the sparse time varying effects of the latent channels. Let $S_\tau(\cdot)$ be the soft thresholding function with a threshold parameter $\tau > 0$, i.e., $S_\tau(x) = \text{sign}(x)(|x| - \tau)I(|x| > \tau)$. Let $\mathcal{N}(\mu, \sigma^2)$ denote the normal distribution with mean μ and variance σ^2 , and $C^+(A)$ denote a half-Cauchy distribution with the scale parameter A . For $p = 1, \dots, T$, we assume

$$\tilde{\beta}_h(t_p) = S_\tau\{\beta_h^*(t_p)\}, \quad \beta_h^*(t_p) = \sum_{l=1}^p \nabla \beta_h^*(t_l), \quad \nabla \beta_h^*(t_l) \sim \mathcal{N}(0, \sigma_h^2), \quad \sigma_h \sim C^+(A), \quad (4)$$

where $\beta_h^*(t_p)$ is the group-level time-varying coefficients before soft-thresholding and $\nabla \beta_h^*(t_p) = \beta_h^*(t_p) - \beta_h^*(t_{p-1})$ represents the difference in the time-varying effects between time points t_p and t_{p-1} . The variance parameter σ_h^2 imposes a global shrinkage on $\nabla \beta_h^*(t_p)$ towards zero, which ensures the time dependence of $\beta_h^*(t)$.

2.2.3 Latent Group Projected Normal Prior

We present prior specifications for the latent group indicators and contribution weights. Let Multinomial($m, \boldsymbol{\nu}$) denote a multinomial distribution with total count m and a vector of probabilities $\boldsymbol{\nu}$. Let $\boldsymbol{\delta}_e = (\delta_{e1}, \dots, \delta_{eH})^\top$ and $\boldsymbol{\alpha}_h = (\alpha_{1h}, \dots, \alpha_{Eh})^\top$. Then we have

$$\boldsymbol{\delta}_e \sim \text{Multinomial}(1, \mathbf{1}_H/H), \quad \boldsymbol{\alpha}_e = \boldsymbol{\alpha}_e^*/\|\boldsymbol{\alpha}_e^*\|_2, \quad \boldsymbol{\alpha}_e^* \sim \mathcal{N}(0, \mathbf{I}_H), \quad (5)$$

where the prior probability of $\delta_{eh} = 1$ is the same across all the latent channels for each channel e ; and $\boldsymbol{\alpha}_h$ follows a projected normal distribution (Wang & Gelfand 2013) with the L_2 -norm being one, i.e., $\|\boldsymbol{\alpha}_e\|_2 = 1$. This prior specification ensures the scale of the time-varying effects at the latent channels are comparable to that at the original EEG channels and thus resolves the model identifiability issue of GLASS.

Figure 3 summarizes the model specifications of GLASS, where the multinomial logistic regression modeling framework presents in (1); and the prior specifications are given in (2) along with (4) and (5). In the following sections, let $\boldsymbol{\theta} = \{[\beta_h^*(t_p)], [\sigma_h], [\delta_{eh}], [\alpha_{eh}^*]\}$ be a collection of all the model parameters and Θ represents the corresponding parameter space. Let $\mathbf{z} = \{z_\kappa\}$ denote the outcome data. Let $\pi(\boldsymbol{\theta})$ represent the prior density of all the parameters. Conditional on the EEG signals $\mathcal{X} = \{\mathbf{X}_\kappa\}$, let $\pi(\mathbf{z}|\boldsymbol{\theta}, \mathcal{X})$ be the likelihood function of $\boldsymbol{\theta}$, $\pi(\mathbf{z}|\mathcal{X}) = \int_{\Theta} \pi(\mathbf{z}, \boldsymbol{\theta}|\mathcal{X})d\boldsymbol{\theta}$ be the marginal likelihood, or the evidence, where $\pi(\mathbf{z}, \boldsymbol{\theta}|\mathcal{X})$ denotes the joint density. $\pi(\boldsymbol{\theta}|\mathbf{z}, \mathcal{X})$ denote the posterior density.

2.3 Posterior Computation

We perform gradient-based variational inference (GBVI) for posterior computation. GBVI combines the power of stochastic optimization and variational inference. GBVI can generally provide accurate point estimations for model parameters and is faster than sampling methods, including Gibbs samplers. The variational inference approximates the true posterior $\pi(\boldsymbol{\theta}|\mathbf{z}, \mathcal{X})$ by seeking a “surrogate” distribution (denoted by q^*) that minimizes the KL-divergence with the true posterior within a distribution family \mathcal{Q} (Blei et al. 2017), i.e., $q^* = \arg \min_{q \in \mathcal{Q}} \text{KL}(q||\pi)$, where $\text{KL}(q||\pi) = \mathbb{E}_q[\log q(\boldsymbol{\theta})] - \mathbb{E}_q[\log \pi(\boldsymbol{\theta}|\mathbf{z}, \mathcal{X})]$. The computation of KL-divergence is difficult as it involves the intractable normalizing constant. However, minimizing the KL-divergence is equivalent to maximizing the evidence

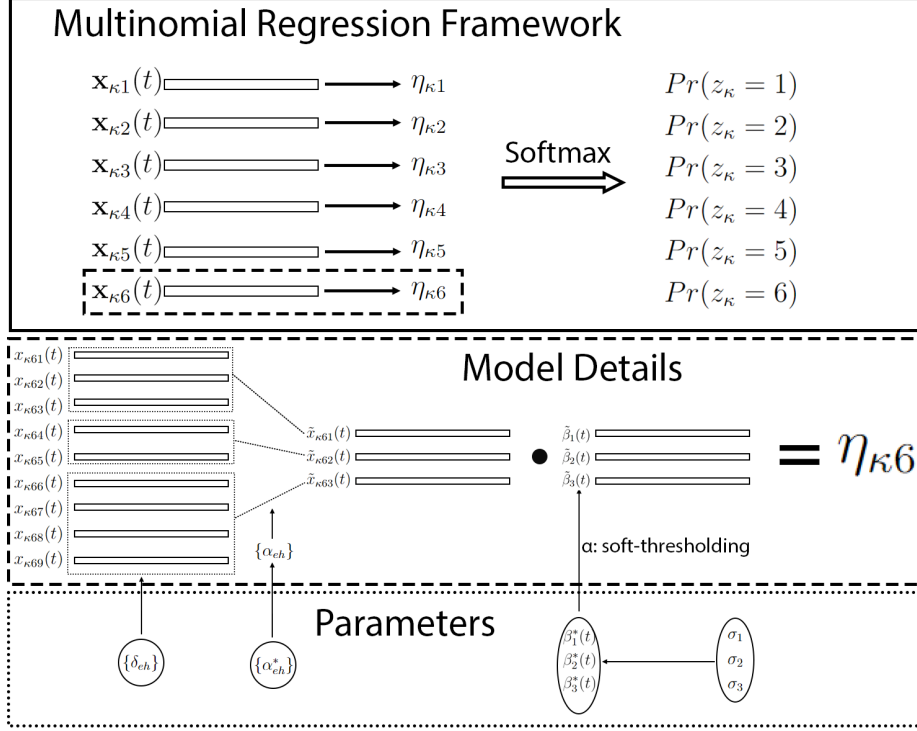


Figure 3: Illustration of GLASS. The first panel illustrates the multinomial regression framework. Based on the extracted EEG series, the model calculates an unnormalized log odds for every stimulus in the half-sequence κ . Those log odds are normalized into probabilities of being the target using the sigmoid function. The second panel shows the following. i) EEG channels are clustered into several latent groups (controlled by the group indicators δ_{eh} 's). ii) each latent group is summarized into one latent channel using linear combinations, with the contribution weights being α_{eh} 's iii) the unnormalized log-odds is the sum of features in latent channels multiplied by the time-varying effects $\tilde{\beta}_h(t)$'s. The third panel displays parameters in GLASS. α_{eh} 's are calculated from α_{eh}^* 's by l_2 -normalization. $\beta_h^*(t)$'s are time-varying effects before the soft-thresholding (cutoff: α), and σ_h 's are scale parameters for time-varying effects specific to each latent channel.

lower bound (ELBO), which is defined as $\text{ELBO}(q) = \mathbb{E}_q[\log \pi(\boldsymbol{\theta}, \mathbf{z}|\mathcal{X})] - \mathbb{E}_q[\log q(\boldsymbol{\theta})]$. Suppose the distribution family \mathcal{Q} is parameterized by $\xi \in U$, where U is an open subset of euclidean space, then $\text{ELBO}(q)$ can be regarded as a function of ξ . To perform gradient-based algorithms, various gradient estimators have been proposed to approximate $\nabla_{\xi}\text{ELBO}(q)$, including i) the score estimator (also known as the log-derivative gradient estimator) (Williams 1992), ii) an extension of i) with reduced variance (Mnih & Rezende 2016), iii) reparameterization gradients as introduced by Kingma & Welling (2013), and iv) doubly-reparameterized estimator presented by Tucker et al. (2018).

In our application study, we adopt iii) reparameterization gradients and the optimizer Adam due to its scalability to large data (Kingma & Ba 2014). In Adam, we set the number of iterations to 2000 and the step size to 0.05. We do not use batch and l_2 -regularization in Adam. In addition, the reparameterization gradient estimator involves Monte Carlo simulation of $\mathbb{E}_q(f)$ for some function f . The number of Monte Carlo samples is set to 10.

2.3.1 Surrogate Distributions

For GLASS, we construct the surrogate distribution as the product of independent distributions, and the distribution family of each parameter is specified as the following.

- $\beta_h^*(t_p)$'s: normal distributions, parameterized by means and variances.
- σ_h 's: log-normal distributions, parameterized by means and variances before the log transformation.
- δ_e 's: relaxed one-hot categorical distributions, parameterized by log-odds.
- α_{eh}^* 's: normal distributions, parameterized by means and variances.

Here, the relaxed one-hot categorical distribution is a continuous approximation of the

multinomial distribution with one total count; it is also introduced as the Gumbel-Softmax (Jang et al. 2016) and Concrete (Maddison et al. 2016) distributions. This is because a continuous parameter space is required for unbiased gradient calculation. Additionally, we use the softplus function, i.e., $f(x) = \log[1 + \exp(x)]$, to map variances to the entire real line to increase the numerical stability.

2.4 Prediction

From the approximate posterior distribution of model parameters, we derive the posterior predictive distribution of the target stimulus given a newly observed sequence of EEG signals. Let κ^* index the new half sequence and \mathbf{X}_{κ^*} be the observed EEG signals. First, the distribution of z_{κ^*} given a fixed model parameter $\boldsymbol{\theta}$ can be expressed as the following.

$$\Pr(z_{\kappa^*} = i \mid \boldsymbol{\theta}, \mathbf{X}_{\kappa^*}) = \frac{\exp(\eta_{\kappa^*i})}{\sum_{i'=1}^6 \exp(\eta_{\kappa^*i'})}, \quad \eta_{\kappa^*i} = \sum_{p=1}^{n_T} \mathbf{x}_{\kappa^*i}^\top(t_p) \boldsymbol{\beta}(t_p). \quad (6)$$

We adopt an importance sampling approach to approximate the posterior predictive distribution of z_{κ^*} using M i.i.d. samples $\{\boldsymbol{\theta}_m\}_{m=1}^M$ from the surrogate distribution q .

$$\begin{aligned} \Pr(z_{\kappa^*} = i \mid \mathbf{z}, \mathcal{X}, \mathbf{X}_{\kappa}) &= \int_{\Theta} \Pr(z_{\kappa^*} = i \mid \boldsymbol{\theta}, \mathbf{z}, \mathcal{X}, \mathbf{X}_{\kappa}) \pi(\boldsymbol{\theta} \mid \mathbf{z}, \mathcal{X}, \mathbf{X}_{\kappa}) d\boldsymbol{\theta} \\ &= \int_{\Theta} \Pr(z_{\kappa^*} = i \mid \boldsymbol{\theta}, \mathbf{X}_{\kappa}) \pi(\boldsymbol{\theta} \mid \mathbf{z}, \mathcal{X}) d\boldsymbol{\theta} \\ &= \int_{\Theta} \Pr(z_{\kappa^*} = i \mid \boldsymbol{\theta}) \frac{\pi(\boldsymbol{\theta}, \mathbf{z} \mid \mathcal{X})}{q(\boldsymbol{\theta}) \pi(\mathbf{z} \mid \mathcal{X})} q(\boldsymbol{\theta}) d\boldsymbol{\theta} \\ &\approx \frac{1}{\pi(\mathbf{z} \mid \mathcal{X}) M} \sum_{m=1}^M \Pr(z_{\kappa^*} = i \mid \boldsymbol{\theta}_m, \mathbf{X}_{\kappa}) \frac{\pi(\boldsymbol{\theta}_m, \mathbf{z} \mid \mathcal{X})}{q(\boldsymbol{\theta}_m)} \end{aligned}$$

Here, $\Pr(z_{\kappa^*} = i \mid \boldsymbol{\theta}, \mathbf{z}, \mathcal{X}, \mathbf{X}_{\kappa}) = \Pr(z_{\kappa^*} = i \mid \boldsymbol{\theta}, \mathbf{X}_{\kappa})$ and $\pi(\boldsymbol{\theta} \mid \mathbf{z}, \mathcal{X}, \mathbf{X}_{\kappa}) = \pi(\boldsymbol{\theta} \mid \mathbf{z}, \mathcal{X})$ by conditional independence assumptions. Notice that $\pi(\mathbf{z} \mid \mathcal{X})$ in the last equation is a normalizing

constant. We can ignore $\pi(\mathbf{z}|\mathcal{X})$ and re-normalize the probabilities into one afterward.

In practice, multiple (say S) 12-stimuli sequences are generated for one character. The S half-sequences (either for rows or columns) $\kappa_1^*, \dots, \kappa_S^*$ will have the same outcome. In this case, we predict the target row or column as the one that maximizes the following conditional probability.

$$Pr(z = i|\mathbf{z}, \mathcal{X}, \{\mathbf{X}_{\kappa_s^*}\}, z_{\kappa_1^*} = \dots = z_{\kappa_S^*} := z) \propto \prod_s^S Pr(z_{\kappa_s^*} = i|\mathbf{z}, \mathcal{X}, \mathbf{X}_{\kappa_s^*})$$

2.5 Channel Importance

We use the Bayes factor to quantify channel importance. The Bayes factor is the evidence ratio of two competing statistical models, where the evidence is defined and estimated by the following.

$$\begin{aligned} m &= \pi(\mathbf{z}|\mathcal{X}) = \int_{\Theta} \pi(\mathbf{z}, \boldsymbol{\theta}|\mathcal{X})\pi(\boldsymbol{\theta})d\boldsymbol{\theta} \\ &= \int_{\Theta} \pi(\mathbf{z}, \boldsymbol{\theta}|\mathcal{X})\frac{\pi(\boldsymbol{\theta})}{q(\boldsymbol{\theta})}q(\boldsymbol{\theta})d\boldsymbol{\theta} \\ &\approx \frac{1}{M} \sum_{m=1}^M \pi(\mathbf{z}, \boldsymbol{\theta}_m|\mathcal{X})\frac{\pi(\boldsymbol{\theta}_m)}{q(\boldsymbol{\theta}_m)} \end{aligned}$$

Here, $\boldsymbol{\theta}_m$'s are M i.i.d. samples from the surrogate distribution q .

We denote the full model by \mathbf{M} . To construct a model \mathbf{M}_{-e} with EEG channel e masked, we replace equation (5) with $\alpha_{e_1h} = \frac{\alpha_{e_1h}^*}{\sqrt{\sum_{e_2 \neq e_1} \alpha_{e_2h}^*{}^2}}$ for $e_1 \neq e$ and $\alpha_{eh} = 0$. In \mathbf{M}_{-e} , channel e can not contribute to any latent channels as α_{eh} 's are intentionally set to zero. Suppose m and m_{-e} are evidence of \mathbf{M} and \mathbf{M}_{-e} , respectively. We define the Bayes factor $B_e := m/m_{-e}$ as the importance index of channel e . Notice that \mathbf{M} and \mathbf{M}_{-e} have the same parameter space. Therefore, the surrogate distribution q can be used as both models'

working density in importance sampling.

The model evidence can be utilized to determine the optimal number of latent groups. Specifically, we fit models with varying numbers of latent groups, e.g. $H \in \{1, 2, 3, 4, 5\}$, and select the one with the highest evidence as the optimal model.

3 Application

We present a real-data application of the GLASS model on a single-participant study (referred to as participant A) and compare it with two competing methods, SWLDA and EEGNet. The data were collected from the P300 keyboard replacement study conducted by the University of Michigan Direct Brain Interface (UMDBI) Laboratory. We chose participant A, a 68-year-old female patient with ALS. Our real-data application involves several steps. First, we fit the GLASS model and determine the optimal number of latent groups using the evidence. Then, we compare the prediction accuracy of GLASS with the two competing methods. Finally, we provide a cross-participant analysis.

3.1 Data Aquisition

We collect data from participant A from 10 BCI sessions. The first session collects the training dataset. In this session, EEG data was recorded while the user focused on each character in “THE QUICK BROWN FOX” (19 characters, including spaces). Each character was repeated for 15 sequences. The nine following sessions are all free-typing sessions that collect the testing dataset. In free-typing sessions, participant A was asked to reproduce a 23-character sentence taped on the top of the screen. Each character was repeated for six sequences. The free-typing was done with correction, i.e., the participant can type the backspace key, one of the 36 keys on the virtual keyboard, when the previous character

was incorrectly typed. During each session, participant A was asked to wear an EEG cap with 16 channels and sit approximately 0.8 m from a 17-inch monitor showing the 6×6 virtual keyboard. The location of the 16 scalp electrodes follows the international 10–20 system, and the channel names are F3, Fz, F4, T7, C3, Cz, C4, T8, CP3, CP4, P3, Pz, P4, PO7, Oz, and PO8. The EEG cap has a sampling rate of 256 Hz. Each stimulus highlighted a row or column for 31.25 milliseconds with a pause of 125 milliseconds before the next row, or column flashed. The time between characters was 3.5 seconds.

We extract 800 milliseconds of EEG signal following each stimulus, corresponding to 205 evenly spaced time points with a 256 Hz sampling frequency. The total number of stimuli is $19 \times 15 \times 12 = 3420$ in the training data and 17640 in the testing data.

3.2 Model Fitting

We fit four GLASS models with $H \in \{1, 2, 3, 4, 5\}$ and use the model evidence to determine the number of latent groups. We set the thresholding parameter α to be 0.001. Computational configurations are mentioned in Section 2.3.

We compared GLASS with two classification methods, SWLDA and EEGNet. Step-wise Linear Discriminant Analysis (SWLDA) is widely used in P300 BCI applications, as introduced by Farwell & Donchin (1988). SWLDA is a modified version of Linear Discriminant Analysis (LDA), which selects a subset of features iteratively to maximize the class separation. To follow the common practice, we set the number of iterations to 64, the max p-value for adding a feature to 0.1, and the minimal p-value for removing a feature to 0.15. SWLDA is typically applied with bandpass filtering and down-sampling for best performance. Therefore, we bandpass filtered the training and testing data for SWLDA between 0.5Hz and 15Hz and downsampled it to 32Hz (8x downsampling) after filtering.

We confirmed that these data processing steps improved the performance of SWLDA. In contrast, EEGNet is a recent deep-learning method Lawhern et al. (2018), which has gained popularity, and the authors provide a reproducible Python module at <https://github.com/aliasvishnu/EEGNet>. We used their default values for hyperparameters in this study. EEGNet takes the raw EEG data without downsampling as input, similar to our proposed method, GLASS.

3.3 Result

The maximum model evidence was achieved with two latent groups. Figure (4) shows the estimated group-level time-varying effects $\tilde{\beta}(t)$, the channel importance (Bayes factor defined in Section 2.5), and the working contribution weights, i.e., $\delta_{eh}\alpha_{eh}$. The first latent group, mainly contributed by Oz, Pz, PO7, and PO8, had more significant time-varying effects than the second latent group. The top 5 most important channels are PO7, PO8, Oz, Pz, and C3. The first group consists of channels in the parieto-occipital region (PO7, PO8, Oz, and Pz) and has a more significant time-varying effect than the second group. The parieto-occipital region is an important brain area for visual processing and attentional control. In the context of brain-computer interfaces (BCIs), the parieto-occipital region is often involved in generating event-related potentials (ERPs) and processing visual stimuli (Takano et al. 2014).

3.4 Character-Level Prediction Accuracy

Figure (5) shows the character-level prediction accuracy of the three methods. Using the maximum number of sequences (15 for the training set and 6 for the testing set), all methods reached a 100% accuracy in the training set, and the character level accuracy in the testing

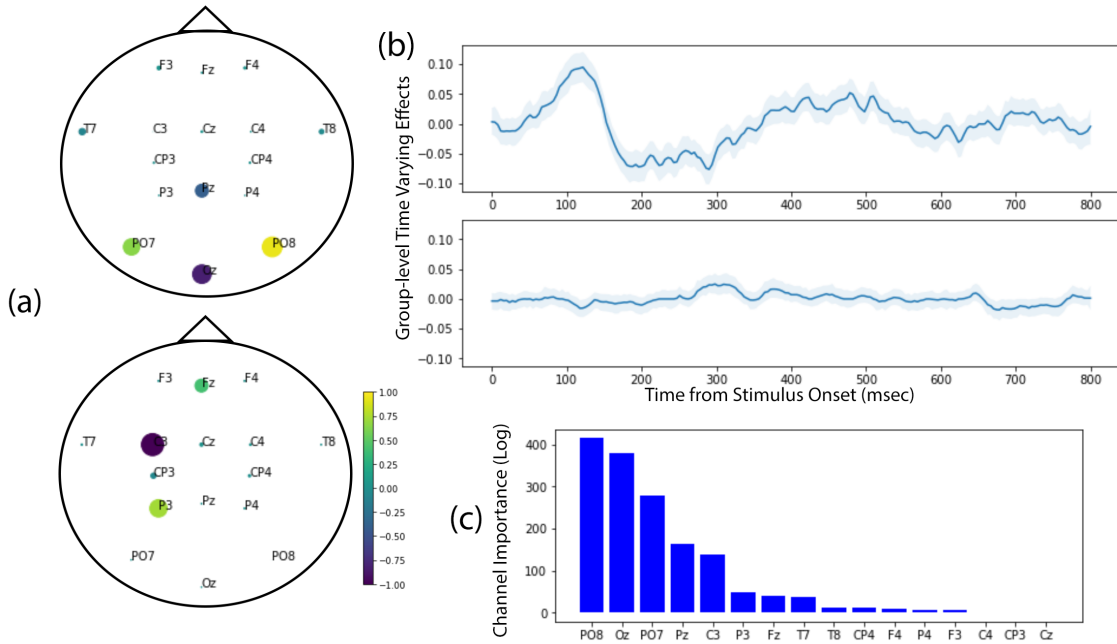


Figure 4: The results obtained from GLASS on participant A. The model evidence was maximized with two latent groups. Subfigure (a) illustrates the working contribution weights of EEG channels to latent groups, visualized on the physical locations of EEG channels on the EEG cap. Subfigure (b) shows the group-level time-varying effects, along with the 95% credit interval. Finally, Figure (c) presents the relative importance of EEG channels quantified by Bayes factors.

set was 93.9%, 84.9%, and 89.8% for GLASS, SWLDA and EEGNet, respectively. Overall, GLASS achieved better prediction accuracy than the two competing methods.

3.5 Cross-participant Study

We applied GLASS to two additional participants, namely participant B and participant C, using the same model configurations described in Section 3.3. Participant B is a 66-year-old male ALS patient with more severe symptoms than participant A, while participant C is a 66-year-old healthy female participant.

Figure (6) displays the results obtained using GLASS on participants B and C. Our findings indicate that GLASS outperformed SWLDA and EEGNet in terms of character-level prediction accuracy on participant B, while the performance was comparable on partic-

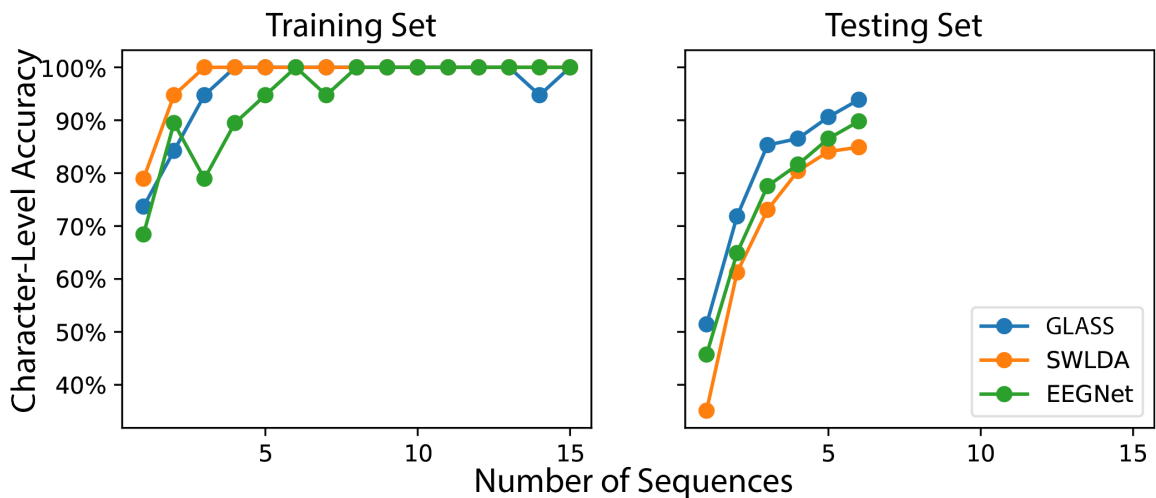


Figure 5: Character-level accuracy of GLASS and the two competing methods in training and testing sets. The x-axis is the number of sequences used for predicting each character.

ipant C. By employing the model evidence, we identified one and two latent groups for participants B and C, respectively. The grouped effect from the parieto-occipital region is replicated in both participants B and C, with similar patterns of contribution weights and time-varying effects. This suggests common EEG mechanisms from the parieto-occipital region shared among participants.

4 Simulation

4.1 Simulation I

In this simulation, we simulate data under assumptions of the GLASS while mimicking the data scale and signal-to-noise ratio of the real data. This simulation aims to test whether GLASS can recover the true latent groups and time-varying effects $\bar{\beta}_{et}$'s. We also test the prediction accuracy of GLASS and compare that to the two competing methods.

We simulate the training data as $|\mathcal{K}| = 1000$ 6-stimuli half-sequences with six stimuli. We generate another set of 1000 half-sequences for testing. The pseudo-EEG series following

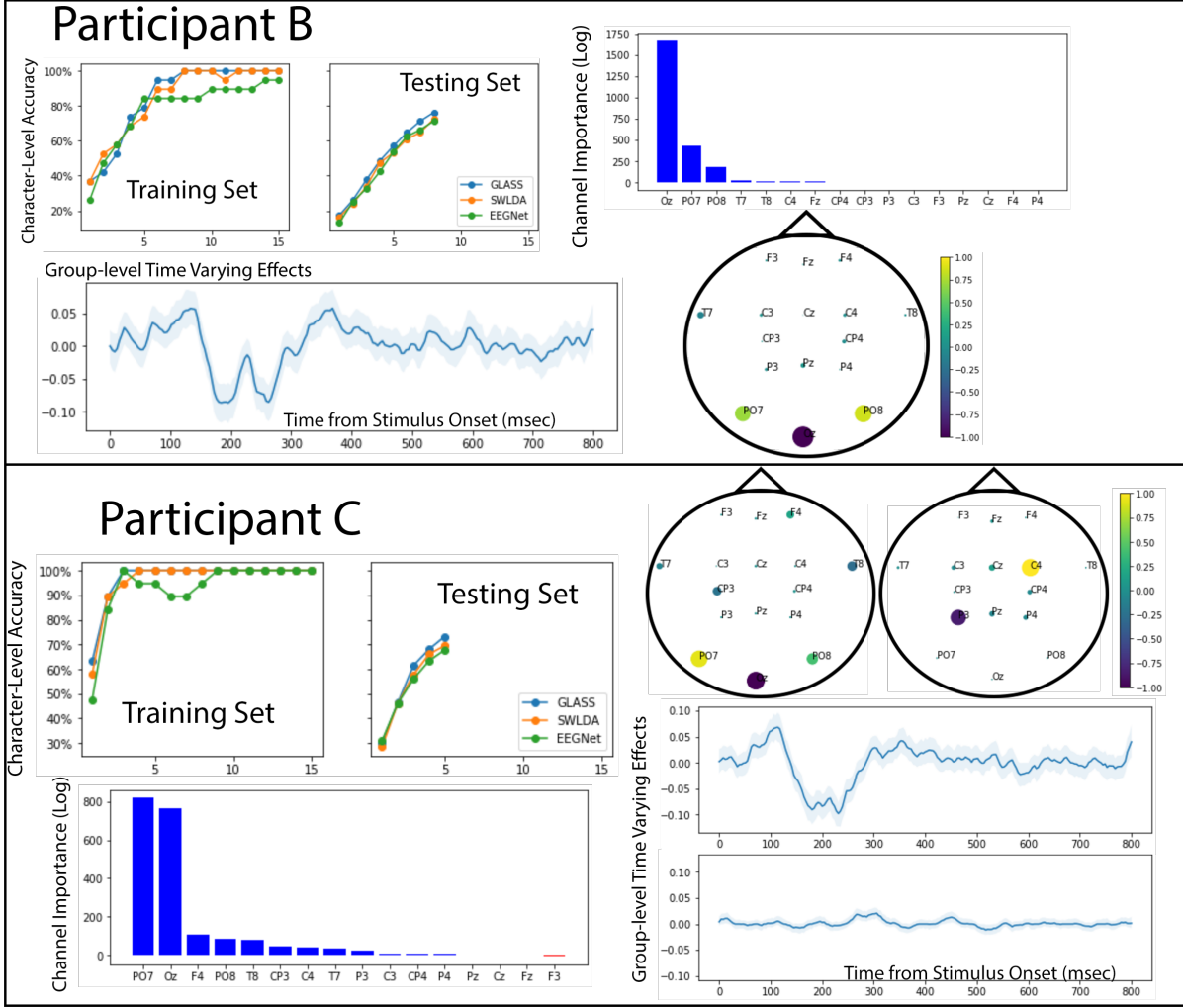


Figure 6: The results obtained from GLASS on participants B and C. Refer to Figure 4 for the meaning of each subfigure in detail.

each stimulus, i.e., $\mathbf{x}_{\kappa i}(t)$, is simulated using $E \times n_T = 16 \times 200$ i.i.d. $N(0, 10^2)$ samples. Here the mean and variance are selected to mimic the distribution of the true EEG signal. We simulate two latent groups containing channels 1-4 and 5-8, respectively. Specifically, $\delta_{e1} = 1$ for $e \in \{1, 2, 3, 4\}$ and $(\alpha_{11}^*, \alpha_{21}^*, \alpha_{31}^*, \alpha_{41}^*) = (1, 1, -1, -1)$ for the first group; and $\delta_{e2} = 1$ for $e \in \{5, 6, 7, 8\}$ and $(\alpha_{52}^*, \alpha_{62}^*, \alpha_{72}^*, \alpha_{82}^*) = (2, 1, -1.5, -1.5)$ for the second group. The remaining eight channels are set to be non-informative, i.e., $\alpha_{eh}^* = 0$ for $e \in \{9, \dots, 16\}$ and $h \in \{1, 2\}$. For the group-level time-varying effect $\tilde{\beta}(t)$, we first evenly map the 200 time points to $[0, 2\pi]$, then generate the true time varying-effects using $0.002\sin(t)$ and

$0.002\sin(t/2)$ for group one and two, respectively. The true soft-thresholding cutoff α is set to 0.001. Channel-wise time-varying effects are visualized as red solid lines in Figure 7. They have similar scales to the real data fitting result.

We replicated the simulation 50 times. In each replication, we fit GLASS, SWLDA, and EEGNet using the training data. The computational configurations of the three methods are set to be the same as in Section 3. We monitor the model evidence of GLASS to determine the number of latent groups from the set $\{1, 2, 3, 4\}$, and we also examine whether informative channels, i.e. channels 1-8, are clustered correctly. We define the following R^2 statistics to evaluate the parameter estimation accuracy of channel-wise time-varying effects $\beta(t)$.

$$R^2 = 1 - \frac{\sum_{p=1}^{n_T} \|\beta(t_p) - \hat{\beta}(t_p)\|^2}{\sum_{p=1}^{n_T} \|\beta(t_p)\|^2} \quad (7)$$

Here, $\hat{\beta}(t_p)$'s are estimated channel-wise time-varying effects, which are calculated by the median of 2000 samples from the surrogate distribution. An R^2 close to one indicates accurate estimation. We evaluate the prediction accuracy of all models on both the training and testing datasets.

The result consistently shows a maximized model evidence with two latent groups in every replication. Also, in each replication, with two latent groups, GLASS correctly clustered channels 1-4 and 5-8 in different latent groups. This demonstrates the consistent clustering accuracy of GLASS. Figure 7 visualizes the true (solid line) and the estimated (dashed line) channel-wise time-varying effects, along with ten random draws from the posterior surrogate distribution in one replication. The mean R^2 across 50 replications is 0.975 (SD: 0.012), demonstrating an accurate estimation of the channel-wise time-varying effects. Table 1 shows the prediction accuracy of the three models. GLASS outperformed both SWLDA and EEGNet in prediction accuracy. Theoretically, no model can have

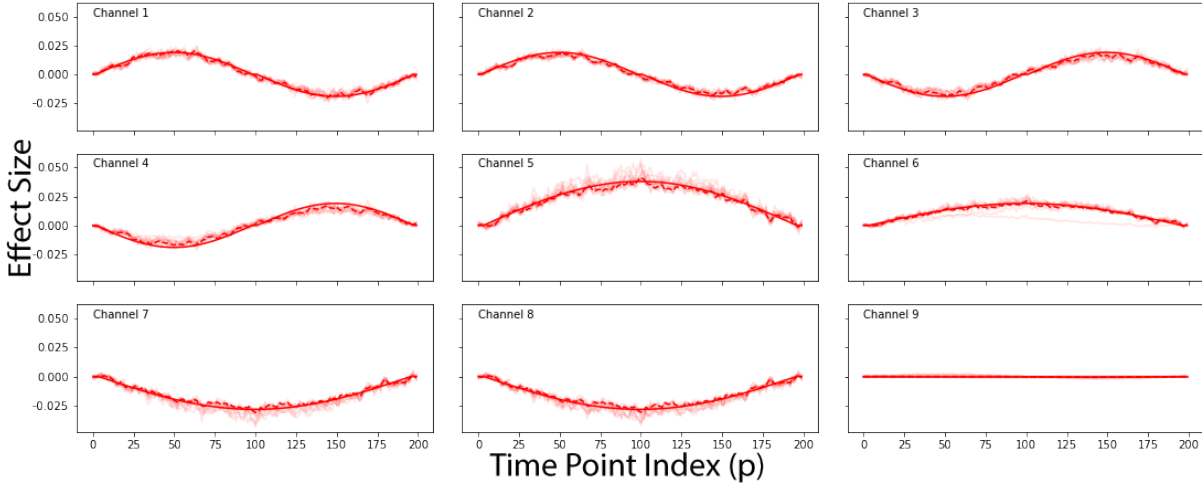


Figure 7: The true (solid line) and the estimated (dashed line) channel-wise time-varying effects, along with ten random draws from the posterior surrogate distribution in one replication. The estimated channel-wise time-varying effects is calculated as the median of 2000 samples from the posterior surrogate distribution.

a higher testing accuracy than that of the true model, evaluated by predicting the labels directly using the multinomial probabilities, i.e., predicting z_κ as the i of the largest $\eta_{\kappa i}$. The mean testing accuracy of 85.1% given by GLASS is very close to the theoretical maximum of 86.8%.

Model	Accuracy (Train)	Accuracy (Test)
GLASS	91.8% (1.0%)	85.1% (1.2%)
SWLDA	44.9% (1.0%)	26.6% (1.7%)
EEGNet	83.6% (1.5%)	80.0% (1.8%)

Table 1: Mean prediction accuracy (standard deviation) of GLASS, SWLDA, and EEGNet over 50 replications. The testing accuracy given by the true model is 86.8%, which is theoretically the maximum testing accuracy that any model can achieve. The testing accuracy of 85.1% given by GLASS is close to that.

4.2 Simulation II

Classification methods should be robust to the inherent variability in human responses to individual stimuli, i.e., they should be robust to difference in distributions of the training and testing data. Latency jitter describes variability in the latency of a person’s ERP

response to each stimulus. Literature has shown how increased latency jitter can cause decreased BCI performance (Thompson et al. 2012, Huggins & Thompson 2016, Mowla et al. 2017). In this simulation study, We impose different levels of artificial latency jitter and random noise on the EEG signals from participant A. We aim to compare the three methods by the reduction in character prediction accuracy on the testing data given different levels of disturbance.

We impose a random time shift to the EEG signal to generate the artificial latency jitter. Suppose $dt \sim N(0, \sigma_t^2)$. We shift the EEG signal by dt milliseconds along the time axis. We independently generate shifts to EEG signals following each stimulus, i.e., $\mathbf{x}_{\kappa i}(t)$. Hence, σ_t^2 determines the level of artificial latency jitter. We add independent $N(0, \tau^2)$ -distributed noises to EEG features. We design three scenarios with $\sigma_t = 5$ and $\tau^2 = 1$ (Scenario I: small disturbance to the testing data), $\sigma_t = 10$ and $\tau^2 = 2$ (Scenario II: moderate disturbance to the testing data), and $\sigma_t = 25$ and $\tau^2 = 5$ (Scenario III: large disturbance to the testing data). We replicated each scenario 50 times. In each replication, we calculated the reduction in character-level prediction accuracy compared to the non-disturbed accuracies reported in Section 3.3.

	GLASS	EEGNet	SWLDA
Scenario I	0.6%(1.1%)	2.8%(1.3%)	20.2%(3.9%)
Scenario II	18.8%(2.2%)	20.2%(2.1%)	52.9%(2.1%)
Scenario III	55.4%(2.2%)	59.9%(2.1%)	63.0%(0.6%)

Table 2: Average reduction (SD) in Character-level accuracy of GLASS, SWLDA, and EEGNet. Scenarios I, II, and III represent the low, moderate, and high levels of artificial disturbance to the testing data, respectively.

Table (2) shows the simulation result. The result shows that GLASS is more robust to latency jitter and noise than the two competing methods as illustrated by less accuracy reduction. Given the higher original prediction accuracy of GLASS (93.9%, 84.9%, and 89.8% for GLASS, SWLDA, and EEGNet, respectively, reported in Section 3.3), the

advantage of being more robust is more pronounced.

5 Conclusion

Using a fully Bayesian framework, we have developed a multivariate regression model with novel prior specifications. Compared to the conventional binary classification in BCI applications, GLASS better represents the generating process of P300 BCI data, thus resolving the dataset imbalance in a model-based manner. The proposed prior specifications enable (i) feature selection and noise reduction using soft thresholding, (ii) smoothing of time-varying effects using global shrinkage, and (iii) alleviating spatial correlation of EEG signals using latent groups. Our method naturally enjoys both model interpretability from Bayesian modeling and efficient computational powered by gradient-based optimization. These improvements are unique and crucial in EEG-based BCI applications and are demonstrated by extensive simulation and application studies.

References

- Blei, D. M., Kucukelbir, A. & McAuliffe, J. D. (2017), ‘Variational inference: A review for statisticians’, *Journal of the American statistical Association* **112**(518), 859–877.
- Ditthapron, A., Banluesombatkul, N., Ketrat, S., Chuangsuwanich, E. & Wilaiprasitporn, T. (2019), ‘Universal joint feature extraction for p300 eeg classification using multi-task autoencoder’, *IEEE Access* **7**, 68415–68428.
- Farwell, L. A. & Donchin, E. (1988), ‘Talking off the top of your head: toward a mental prosthesis utilizing event-related brain potentials’, *Electroencephalography and clinical Neurophysiology* **70**(6), 510–523.

- Huggins, J. E. & Thompson, D. E. (2016), P300 latency jitter more likely for people with
als, *in* ‘Proceedings of the 6th International Brain-Computer Interface Meeting, organized
by the BCI Society’, p. 58.
- Jang, E., Gu, S. & Poole, B. (2016), ‘Categorical reparameterization with gumbel-softmax’,
arXiv preprint arXiv:1611.01144 .
- Joshi, R., Goel, P., Sur, M. & Murthy, H. A. (2018), Single trial p300 classification using
convolutional lstm and deep learning ensembles method, *in* ‘International Conference on
Intelligent Human Computer Interaction’, Springer, pp. 3–15.
- Kingma, D. P. & Ba, J. (2014), ‘Adam: A method for stochastic optimization’, *arXiv
preprint arXiv:1412.6980* .
- Kingma, D. P. & Welling, M. (2013), ‘Auto-encoding variational bayes’, *arXiv preprint
arXiv:1312.6114* .
- Krusienski, D. J., Sellers, E. W., Cabestaing, F., Bayouth, S., McFarland, D. J., Vaughan,
T. M. & Wolpaw, J. R. (2006), ‘A comparison of classification techniques for the p300
speller’, *Journal of Neural Engineering* **3**(4), 299.
- Lawhern, V. J., Solon, A. J., Waytowich, N. R., Gordon, S. M., Hung, C. P. & Lance, B. J.
(2018), ‘Eegnet: a compact convolutional neural network for eeg-based brain–computer
interfaces’, *Journal of neural engineering* **15**(5), 056013.
- Ma, T., Li, Y., Huggins, J. E., Zhu, J. & Kang, J. (2022), ‘Bayesian inferences on neu-
ral activity in eeg-based brain-computer interface’, *Journal of the American Statistical
Association* **117**(539), 1122–1133.

- Maddison, C. J., Mnih, A. & Teh, Y. W. (2016), ‘The concrete distribution: A continuous relaxation of discrete random variables’, *arXiv preprint arXiv:1611.00712* .
- Mnih, A. & Rezende, D. (2016), Variational inference for monte carlo objectives, *in* ‘International Conference on Machine Learning’, PMLR, pp. 2188–2196.
- Mowla, M. R., Huggins, J. E. & Thompson, D. E. (2017), ‘Enhancing p300-bci performance using latency estimation’, *Brain-Computer Interfaces* **4**(3), 137–145.
- Philip, J. T. & George, S. T. (2020), ‘Visual p300 mind-speller brain-computer interfaces: a walk through the recent developments with special focus on classification algorithms’, *Clinical EEG and Neuroscience* **51**(1), 19–33.
- Takano, K., Ora, H., Sekihara, K., Iwaki, S. & Kansaku, K. (2014), ‘Coherent activity in bilateral parieto-occipital cortices during p300-bci operation’, *Frontiers in neurology* **5**, 74.
- Thompson, D. E., Warschausky, S. & Huggins, J. E. (2012), ‘Classifier-based latency estimation: a novel way to estimate and predict bci accuracy’, *Journal of Neural Engineering* **10**(1), 016006.
- Tucker, G., Lawson, D., Gu, S. & Maddison, C. J. (2018), ‘Doubly reparameterized gradient estimators for monte carlo objectives’, *arXiv preprint arXiv:1810.04152* .
- Wang, F. & Gelfand, A. E. (2013), ‘Directional data analysis under the general projected normal distribution’, *Statistical methodology* **10**(1), 113–127.
- Williams, R. J. (1992), ‘Simple statistical gradient-following algorithms for connectionist reinforcement learning’, *Reinforcement learning* pp. 5–32.